IEEE Photonics Journal
An IEEE Photonics Society Publication

Open Access

Joint Modulation Format Identification and Frequency Offset Estimation Based on Superimposed LFM Signal and FrFT

Volume 11, Number 5, October 2019

Yuxiao Guo
Muguang Wang, *Member, IEEE*
Yaozu Li
Hongqian Mu
Beilei Wu
Yan Liu
Fengping Yan

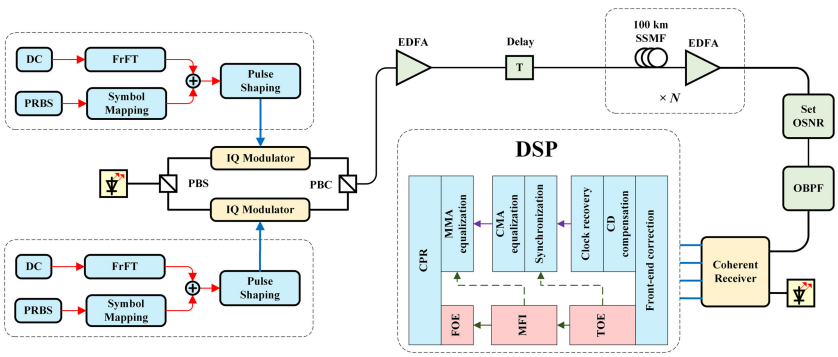

DOI: 10.1109/JPHOT.2019.2944064

Joint Modulation Format Identification and Frequency Offset Estimation Based on Superimposed LFM Signal and FrFT

Yuxiao Guo, Muguang Wang, *Member, IEEE*, Yaozu Li, Hongqian Mu, Beilei Wu, Yan Liu, and Fengping Yan

Institute of Lightwave Technology, Key Laboratory of All Optical Network and Advanced Telecommunication Network, Ministry of Education, Beijing Jiaotong University, Beijing 100044, China

DOI:10.1109/JPHOT.2019.2944064

Manuscript received July 23, 2019; revised September 17, 2019; accepted September 23, 2019. Date of publication October 3, 2019; date of current version October 9, 2019. This work was supported in part by the National Natural Science Foundation of China under Grants 61775015, 61475015, 61801017, 61975009, and 61827818, and in part by the Fundamental Research Funds for the Central Universities under Grant 2018JBZ109. Corresponding author: Muguang Wang (email: mgwang@bjtu.edu.cn).

Abstract: We propose a novel technique for joint modulation format identification and frequency offset (FO) estimation. The linear frequency modulation signal which is obtained by a direct current signal and Fractional Fourier Transform (FrFT) is superimposed on the data symbols to mark and identify the modulation formats. Simulation results demonstrate our method can identify the DPBPSK, DPQPSK, DP8PSK, DP16QAM, DP32QAM and DP64QAM modulation formats correctly before chromatic dispersion compensation even the optical signal to noise ratio is extremely low. Additionally, due to the excellent time and frequency analysis properties of FrFT, the FO estimation range is greatly extended compared with the traditional Viterbi-Viterbi method.

Index Terms: Modulation format identification, Frequency offset estimation, Linear frequency modulation, Fractional Fourier Transform.

1. Introduction

The emergence of novel data services such as 5G and internet of things brings great challenge to the current optical network. In order to address this challenge, elastic optical networks (EON) are introduced to maximize the network resource [1], [2]. In such EON, flexible transceiver which can adjust the modulation formats according to the network traffic is equipped. Hence the modulation format identification (MFI) technique is indispensable for the allocation of network resources and modulation format dependent digital signal processing (DSP) algorithms.

To achieve efficient MFI, many relevant methods have been proposed. In [3], [4], the amplitude histograms or power distributions were used to distinguish the modulation formats. However, these methods are not suitable for the phase shift keying (PSK) systems due to the vacancy for the phase information. MFI can also be achieved in Stokes space [5]–[9], which can monitor the modulation formats accurately in both quadrature amplitude modulation (QAM) systems and PSK systems. But this technique may be a little bit complex and it is vulnerable to the amplified spontaneous emission (ASE) noise. Deep learning and image processing based method may be a kind of popular way in the future but it is impractical due to the current limitation of computation power [10]–[12].

Furthermore, the MFI method based on the sub-carrier pilot was proposed in [13]. It is valid even for the more complex modulation formats such as time hybrid QAM and multi-dimensional formats. However, it will sacrifice the spectral efficiency because of the inserted pilot sequence. Another MFI method enabled by digital frequency offset (FO) loading technique was demonstrated in [14]. It can support more complex modulation formats without spectral efficiency reduction. Yet all these MFI methods mentioned above must be conducted after the chromatic dispersion (CD) compensation or constant modulus algorithm (CMA) equalization. Therefore, the subsequent DSP flows including multi modulus algorithm (MMA) equalization, FO estimation and carrier phase recovery (CPR) has to stop when MFI is in progress because these procedures can't work without the modulation format information. If an MFI method can be conducted before CD compensation, DSP procedures could be optimized by parallel processing technique. For example, the MFI and CMA equalization could be conducted simultaneously rather than sequentially. Hence the total execution time will be greatly saved.

In this paper, an MFI method before CD compensation is proposed based on the Fractional Fourier Transform (FrFT) which has been widely used in CD estimation, interchannel nonlinearity estimation, as well as the time / frequency synchronization [15]–[21]. We successfully used the FrFT and linear frequency modulation (LFM) signal to achieve an effective MFI. Meanwhile, the FO is estimated with the deviation between the peak and middle position in fractional domain. It is illuminated by simulation that the proposal can recognize the common used modulation formats: DPBPSK (Dual Polarization Binary Phase Shift Keying), DPQPSK (Dual Polarization Quad Phase Shift Keying), DP8PSK (Dual Polarization 8-ary Phase Shift Keying), DP16QAM (Dual Polarization 16-ary Quadrature Amplitude Modulation), DP32QAM (Dual Polarization 32-ary Quadrature Amplitude Modulation) and DP64QAM (Dual Polarization 64-ary Quadrature Amplitude Modulation) even when the OSNR drops down to a very low value. In addition, the FO estimation range is approximately extended to $[-R_s/2, +R_s/2]$ (R_s means the symbol rate) in theory and the absolute value of estimation error is less than 2 MHz when the FO is in the range of $[-5$ GHz, 5 GHz$]$.

2. Principle

2.1 LFM Signal Generation by DC Signal and FrFT

The FrFT of a signal $x(t)$ can be described through its integral kernel K_p:

$$F^{\alpha}(u) = \int_{-\infty}^{+\infty} x(t) K_p(u,t) dt \tag{1}$$

$$K_p(u,t) = \begin{cases} \sqrt{1 - j\cot\alpha}\exp\left[j\pi(u^2\cot\alpha - 2ut\csc\alpha + t^2\cot\alpha)\right], & \alpha \neq \mathrm{n}\pi \\ \delta(t+u), & \alpha = (2n \pm 1)\pi \\ \delta(t-u), & \alpha = 2\mathrm{n}\pi \end{cases} \tag{2}$$

$$\alpha = \frac{p\pi}{2} \tag{3}$$

where p is the order of FrFT, α is the rotation angle in Wignar Plane (Time-Frequency Plane) [22], [23]. Apparently, FrFT will change into conventional Fourier Transform when the order $p = 1$ (or the rotation angle $\alpha = \frac{\pi}{2}$).

LFM signal is a special signal whose frequency varies linearly with time. It can be expressed as:

$$x(t) = \exp[j(\varphi_0 + 2\pi f_0 + \pi k t^2)] \tag{4}$$

where φ_0 is the initial phase, f_0 is the carrier frequency, and k is the chirp rate. For a digitalized LFM signal, there exists a peak in fractional domain if the optimal order is chosen. As is derived in [16], the optimal order is shown below:

$$p_{opt} = 1 + \frac{\arctan[(Tf_s - 1)k/f_s]}{\pi/2} \tag{5}$$

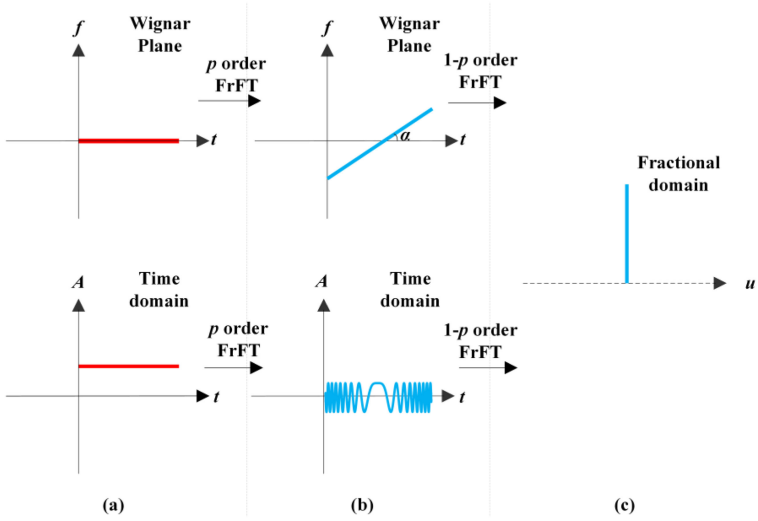

Fig. 1. LFM generation process and fractional domain profile after the optimal order FrFT. (a) DC signal in Wignar Plane and time domain. (b) LFM signal in Wignar Plane and time domain. (c) LFM signal in fractional domain after the optimal order FrFT.

where T and f_s is the sampling time and frequency of the digital signal.

In Wignar Plane, a slope line corresponds to an LFM signal while the line in coincidence with t-axis corresponds to a direct current (DC) signal. Since FrFT can induce rotations in Wignar domains [22], [23], the LFM signal whose carrier frequency is zero can be obtained by a DC signal with the aid of FrFT. As is shown in Fig. 1, after a p order FrFT, the DC signal $d(t)$ will become an LFM signal:

$$S_p(t) = FrFT(d(t), p) \tag{6}$$

where $S_p(t)$ denotes the LFM signal in time domain and we call the subscript p as the order of LFM signal for brevity. If a $1-p$ order FrFT is operated on $S_p(t)$, the LFM signal will converge into a peak of pulse signal in the middle position of fractional domain. Accordingly, the optimal order of FrFT is $1-p$ for an LFM signal whose order is p.

Typically, chirp rate is the most important parameter of LFM signal. Hence it is necessary to analyze the chirp rate of $S_p(t)$. The absolute value of the chirp rate can be expressed as:

$$|k| = \frac{Baud \times \tan\left(\frac{\pi}{2} \times |p|\right)}{T} \tag{7}$$

where $Baud$ is the Baud rate in the system and T is the duration of LFM signal. It can be found the chirp rate is related to the order and duration of the signal.

2.2 MFI by FrFT

To achieve blind MFI, a mapping rule between modulation formats and the orders of LFM signals should be established beforehand. As is shown in Table 1, the modulation formats in a system are represented by $[m_1, m_2, m_3 \ldots]$ and the corresponding LFM signal orders are denoted as $[p_1, p_2, p_3 \ldots]$. These LFM signals are recorded as:

$$[S_{p_i}] \quad i = 1, 2, 3 \ldots \tag{8}$$

Clearly, the optimal orders of FrFTs for these LFM signals are $[1-p_1, 1-p_2, 1-p_3 \ldots]$. For the modulation format marked as m_j, the LFM signal S_{p_j} is superimposed on the symbols after

TABLE 1
Mapping Rules Between Modulation Formats and the Orders of LFM Signals and the Corresponding Optimal Orders of FrFT

Modulation formats	m_1	m_2	m_3	$...m_i$
Corresponding orders of LFM signals	p_1	p_2	p_3	$\cdots p_i$
Optimal orders of FrFT	$1-p_1$	$1-p_2$	$1-p_3$	$...1-p_i$

modulation symbol mapping. Thus the transmitted symbol sequence $t_j(n)$ is expressed as:

$$t_j(n) = m_j(n) + S_{p_j}(n) \quad n = 1, 2, 3 \ldots \tag{9}$$

After transmission, the received signal is down-sampled as 1 sample/symbol before the CD compensation. The down-sampled signal $r_j(n)$ can be expressed as:

$$r_j(n) = m'_j(n) + S'_{p_j}(n) + N(n) \quad n = 1, 2, 3 \ldots \tag{10}$$

where $m'_j(n)$ is the received data symbol, $N(n)$ is the additional ASE noise and $S'_{p_j}(n)$ is the received LFM component after transmission. We operate FrFTs on the down-sampled signal with the orders $[1 - p_1, 1 - p_2, 1 - p_3 \ldots]$ respectively and the results are expressed as:

$$R_i = FrFT(r_j, 1 - p_i) \quad i = 1, 2, 3 \ldots \tag{11}$$

For the modulation format m_j, there will exist a peak which corresponds to the LFM component and a flat pedestal which corresponds to the data and ASE noise in the fractional domain after the $1 - p_j (i = j)$ order FrFT. However, the peak will disappear when the order is not $1 - p_j (i \neq j)$. So the modulation format m_j can be determined by the order of FrFT when a peak is detected. Peak detection can be performed according to the peak to average power rate (PAPR) [24]:

$$PAPR = \frac{\max(|R_i|^2)}{(\overline{|R_i|^2})} \; i = 1, 2, 3 \ldots \tag{12}$$

Apparently, the PAPR will be the biggest when the transformation order is $1 - p_j$ because there will be a peak in fractional domain. Consequently, the modulation format can be determined by the order of FrFT when the PAPR is the biggest. The optimal order corresponding to the modulation format m_j can be determined by:

$$1 - p_j = \underset{1-p_i, i=1,2,3...}{\arg} \max(PAPR) \tag{13}$$

When the optimal order is determined, the modulation format can be found through looking up table method [25].

For example, supposing a system supports DPBPSK, DPQPSK, DP8PSK, DP16QAM, DP32QAM and DP64QAM, then we could assign the LFM signals to the modulation formats according to Table 2. The LFM signal is superimposed on the symbols after symbol mapping. The obtained sequence goes through the pulse shaping filter and is modulated on the optical carrier by IQ modulator. After transmission, the received signal is downsampled and operated by [0.99, 0.985, 0.98, 0.975, 0.97, 0.965] order FrFTs. Subsequently, each PAPR of the six obtained signals after FrFTs is calculated and the biggest PAPR is chosen to check its corresponding order of FrFT. Then the modulation format can be determined through looking up table. In this example, if the optimal order to the biggest PAPR is 0.99, the modulation will be DPBPSK, and other relationships between optimal orders and modulation formats are shown in Table 2.

TABLE 2
Example of Mapping Relationships Among Modulation Formats, Orders of LFM Signals and the Optimal Orders of FrFTs

Modulation Formats	DPBPSK	DPQPSK	DP8PSK	DP16QAM	DP32QAM	DP64QAM
Orders of LFM signal	0.01	0.015	0.02	0.025	0.03	0.035
Optimal orders of FrFT	0.99	0.985	0.98	0.975	0.97	0.965

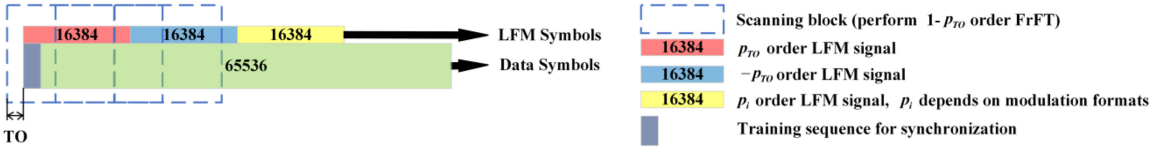

Fig. 2. Frame structure and the process to find the rough location of frame head. (TO: time offset.)

2.3 FO Estimation Enabled by FrFT

The received LFM component $S'_{p_j}(n)$ can be further expressed as:

$$S'_{p_j}(n) = S_{p_j}(n)\exp(2\pi\Delta f n T_s) \quad n = 1, 2, 3\ldots \tag{14}$$

where Δf indicates the FO and T_s means the sampling interval. From Eq. (14), the FO is equivalent to the carrier frequency of received LFM signal. Clearly, the peak will be on the middle position of fractional axis after an optimum order FrFT if Δf is zero. However, the position will deviate from the center if Δf is nonzero. That means the deviation can be employed to estimate FO. The detail relationship between FO and peak deviation is expressed as [21]:

$$\Delta f = \frac{u - u_{mid}}{cos(p_j\pi/2)} \cdot df \tag{15}$$

$$df = \frac{R_s}{N} \tag{16}$$

where u is the position of the peak, u_{mid} is the middle position, df is the frequency resolution, R_s is the symbol rate and N is the length of LFM signal. It should be noted that p_j is the order of superimposed LFM signal not the optimal order of FrFT. The maximum deviation of the peak is $N/2$, which limits the FO estimation range in the interval $[-R_s/2\,cos(p_j\pi/2), +R_s/2\,cos(p_j\pi/2)]$. As Table 2 shows, the order p_j is close to 0, so the FO estimation range based on this approach is approximately to $[-R_s/2, +R_s/2]$.

2.4 Frame Head Location Searching Method

It is noted that our MFI and FO method will be invalid if the head of the superimposed LFM signal can't be found. We take a time synchronization method based on FrFT detailed in [20], [21] to estimate the frame head location with negligible errors. In our scheme, the frame structure can be devised as Fig. 2. For brevity, the length of a frame is set to 65536 symbols which include 128 symbols for synchronization and the frame is averagely divided into four parts. For the first part, an LFM signal with a known order p_{TO} is superimposed and the second part is superimposed with an LFM signal with the order $-p_{TO}$. These two parts are used to estimate the frame head location and the subsequent synchronization. The third part is superimposed with the LFM signal whose order is decided by the modulation format while the last part is superimposed with nothing.

At receiver, the rough location of frame head is found by scanning the received signal step by step to find the peak after a $1 - p_{TO}$ order FrFT. The scanning block contains N symbols and the

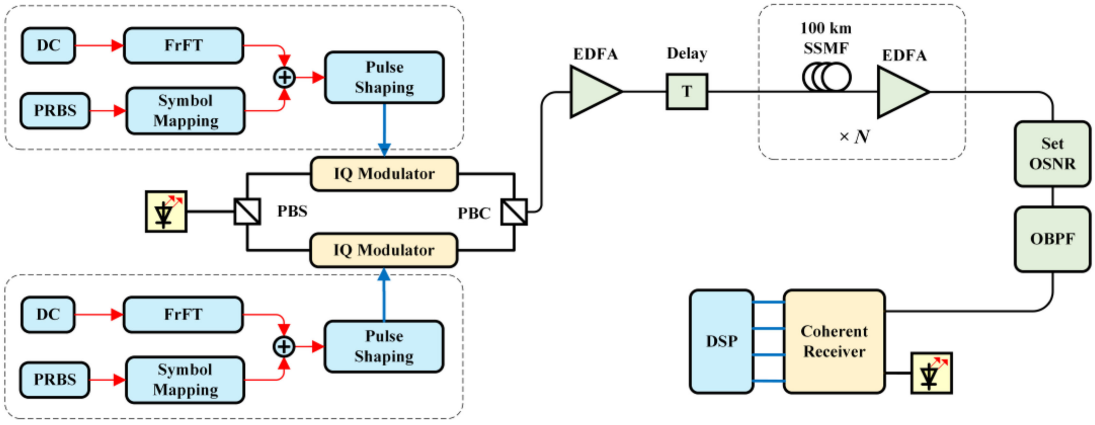

Fig. 3. Schematic of the system setup. (PBS: polarization beam splitter, PBC: polarization beam combiner.)

step size is set to $N/2$ (N is the length of LFM and is set to be 16384 symbols in this paper) to ensure the frame head location can be found in a low OSNR. When the first peak is detected at the k times scanning, we extract the N symbol sequence starting from the place $TT + N$, where TT is the current scanning block head and can be calculated by $TT = (k-1) \times N$. The deviation between the peak and middle position in fractional domain is denoted as $u1$. Then we performed a $-(1 - p_{TO})$ order FrFT on the extracted symbols and the peak deviation is denoted as $u2$. So the time offset (TO) can be estimated by:

$$TO = \frac{u1 + u2}{2\sin(p_{TO} \cdot \pi/2)} \tag{17}$$

Finally, the frame head location FH can be determined by the estimated rough location of frame head and TO using the equation: $FH = TT + TO$. And the third part of the frame can be extracted to perform the MFI and FO estimation by the abovementioned method.

3. System Setup and Results

3.1 System Setup

In order to validate our method, a simulation experiment is performed via OptiSystem and MATLAB as is shown in Fig. 3. Six modulation formats in Table 2 are used in our simulation and the symbol rate is 28 GBaud. The frame structure is composed of 65536 symbols whose structure is shown in Fig. 2. p_{TO} is set to be 0.05 and the order in third part is shown in Table 2. After superimposing the corresponding LFM signal on the mapping symbols and pulse shaping, the electric signal is modulated by a dual polarization IQ modulator and CW laser whose linewidth is set to be 100 kHz. Then the optical signal is amplified by an erbium-doped fiber amplifier (EDFA) and transmitted over a fiber recirculating loop comprising of a 100 km span of standard single-mode fiber (SSMF) and an inline EDFA which is used to compensate the loss of SSMF. The CD and nonlinear coefficient of SSMF are 16.75 ps/(nm · km) and 1.31 $W^{-1}km^{-1}$ respectively. At the end of the loop, additional noise is added to adjust the OSNR while an optical band pass filter (OBPF) is used to eliminate the out-of-band noise. Finally, the optical signal is received by a coherent receiver and the DSP is used to recover and decode the signal. The TO is set in the Delay module by changing the value of delay time and the FO is set by changing the central frequency of the laser in coherent receiver.

The traditional DSP algorithms for a multi-modulation format system include normalization, re-sampling, I/Q correction, CD compensation, synchronization, CMA equalization, MFI, MMA equalization (Radius-Directed Algorithm) as well as FO estimation and CPR serially. It can be seen that

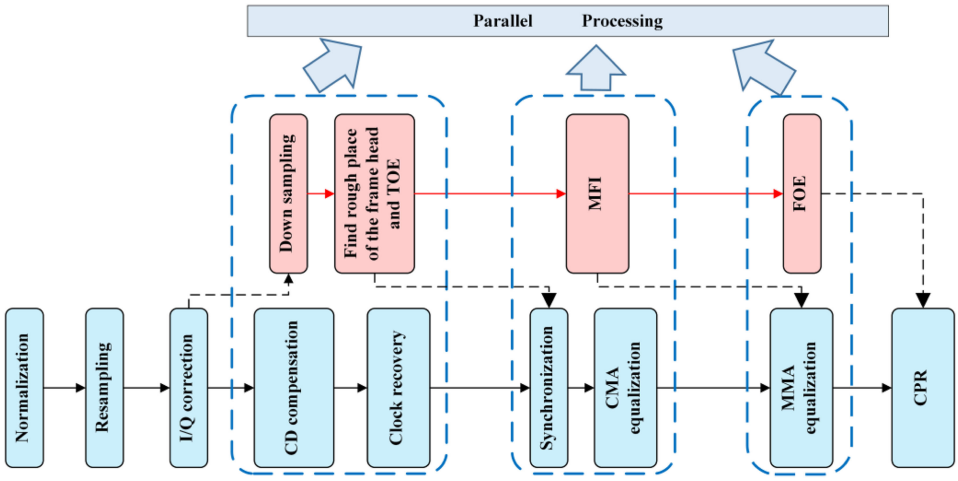

Fig. 4. DSP flows at receiver optimized by the parallel processing. (TOE: TO estimation, FOE: FO estimation.)

TABLE 3
PR Used in the Simulation

Modulation formats	DPBPSK	DPQPSK	DP8PSK	DP16QAM	DP32QAM	DP64QAM
PR (dB)	25	25	26	27	28	28

when MFI is performing, the subsequent DSP flows have to stop. Thanks to the CD insensitivity of our method, the DSP algorithm can be optimized by parallel processing. As is shown in Fig. 4, the DSP flow can be dived into two parallel parts. The TO estimation and CD compensation as well as the clock recovery can be conducted simultaneously, and MFI can be performed with synchronization and CMA equalization. In the same way, FO estimation can be conducted with MMA equalization. The TO estimation result can be used to simplify the synchronization process [21]. The MFI result can be used in the MMA equalization and the FO estimation result can be used for CPR. By the parallel processing, the total DSP execution time will be greatly saved.

3.2 BER Performance Comparison With and Without the Superimposed LFM Signal

Due to the superimposed LFM signal, the bit error ratio (BER) performance will be degraded theoretically. In order to ensure a better BER performance, the power of LFM signal should be as low as possible. However, a lower power will be harder to identify and the LFM signal may be drowned in the data and noise. Therefore, choosing the power ratio *PR* between the data signal and LFM signal is a trade-off between BER and MFI performance. In order to get a good result both in the BER and MFI performance, extensive simulations are conducted and the *PR* is optimized as shown in Table 3.

First the back-to-back (B2B) BER performance is investigated. As is shown in Fig. 5(a), for the low order modulation formats include DPBPSK, DPQPSK, DP8PSK and DP16QAM, all the OSNR penalties due to the superimposed LFM signal at FEC threshold are less than 0.5 dB, which means that the negative effects can be neglected. While the penalties are approximately 0.7 dB for DP32QAM and 1.4 dB for DP64QAM, which also can be acceptable in real system. Then the system performances after transmission (1800 km for DPBPSK, 1600 km for DPQPSK, 1400 km for DP8PSK, 1200 km for DP16QAM, 400 km for DP32QAM and DP64QAM) are also investigated. As is shown in Fig. 5(b), the similar conclusions can be conducted as the B2B systems, which verifies that our scheme is completely feasible in practice.

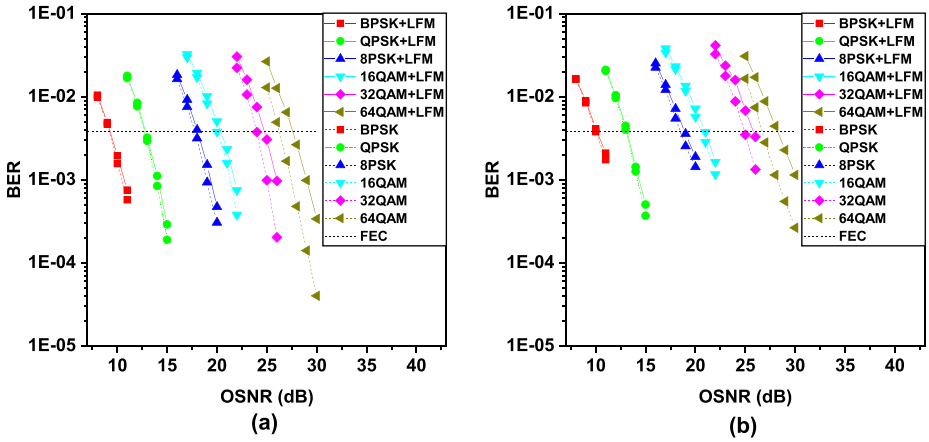

Fig. 5. BER comparison with and without the superimposed LFM signal in different OSNRs: (a) B2B, (b) after transmission (1800 km for DPBPSK,1600 km for DPQPSK, 1400 km for DP8PSK, 1200 km for DP16QAM, 400 km for DP32QAM and DP64QAM).

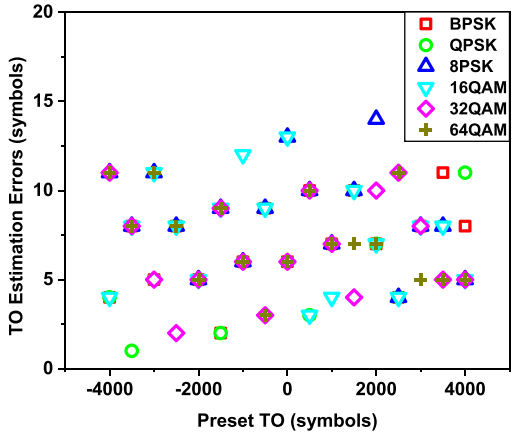

Fig. 6. TO estimation errors.

3.3 TO Estimation Performance

Just as explained before, finding the frame head location accurately is the premise of follow-up MFI and FO estimation. Due to the scanning step is 8192 symbols, the absolute value of maximum TO should be 4096. So the TO from −4000 to 4000 symbols at a step of 500 symbols is set in advance for six modulation formats when an FO of 5 GHz is in existence and OSNRs are 6 dB for DPBPSK and DPQPSK, 8 dB for DP8PSK, 10 dB for DP16QAM, 12 dB for DP32QAM and DP64QAM. In order to get a more stable result, we use the summation of fractional spectrums of two polarizations. Fig. 6 depicts the TO estimation errors. The maximum errors are less than 20 symbols for all the modulation formats. Clearly, even in a very low OSNR and large FO condition, the TO estimation performance is still good enough for the subsequent operations.

3.4 MFI Results

After TO estimation, the frame head location is estimated and the third superimposed LFM signal can be extracted for MFI and FO estimation. To demonstrate the proposed MFI method can still work in bad conditions, we set the FO to 5 GHz and the TO to 4000 symbols. In our method, the corresponding order of a modulation format can be determined by Eq. (13). Then the modulation format can be identified by look-up table.

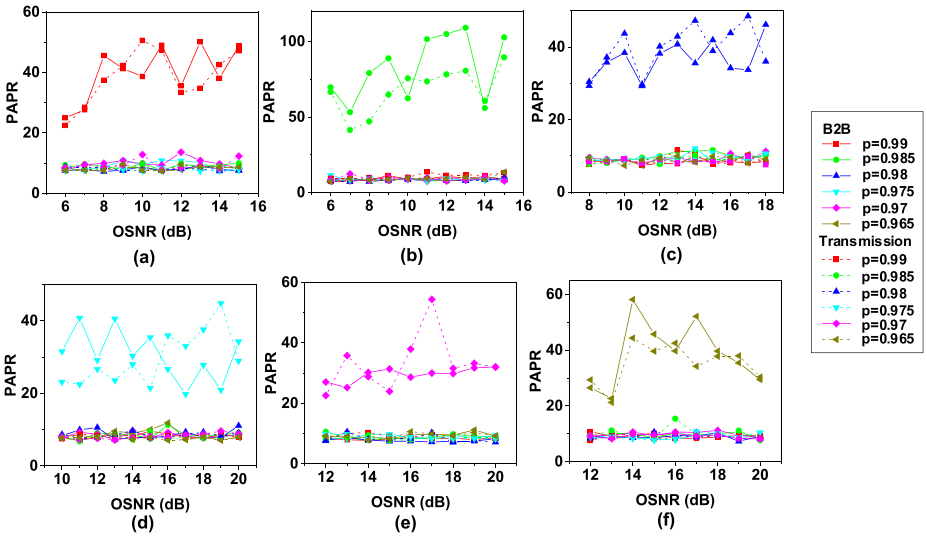

Fig. 7. The PAPR values versus OSNRs for (a) DPBPSK; (b) DPQPSK; (c) DP8PSK; (d) DP16QAM; (e) DP32QAM; (f) DP64QAM.

Fig. 7 shows the PAPRs after different order FrFTs for each modulation format. The solid lines correspond to B2B conditions while the dashed lines are for transmission cases (the transmission distances are the same as what second 3.2 describes). Clearly, for a modulation format, the PAPR will be the biggest when the optimal order is taken. It can be seen from Fig. 7 that the biggest PAPR is obtained when the order is 0.99 for DPBPSK, 0.985 for DPQPSK, 0.98 for DP8PSK, 0.975 for DP16QAM, 0.97 for DP32QAM and 0.965 for DP64QAM. Apparently, our MFI method has a relatively strong resistance to ASE noise. Even in a very low OSNR regime, our proposal still has a good identification performance. Incidentally, as the OSNR increase, the biggest PAPR profile seems not to show a linear increasing trend. The reason is that the contribution of different data and noise to the peak value may be different. Moreover, our method has the potential to support more types and more complex modulation formats.

To further investigate the influence of fiber nonlinearity to the MFI performance, we change the launch power from -2 dBm to 4 dBm, in a step of 1 dBm. The link length is set as the second 3.2 describes and the noise figure of each EDFA is set to be 4 dB. Fig. 8 shows the PAPR versus the launch power. It can be found when the launch power increases, the transformation orders corresponding to biggest PAPRs of each modulation format won't change, which demonstrates our MFI method has a strong robustness to fiber nonlinearity.

3.5 FO Estimation Results

FO can be estimated according to the difference between the peak and middle position in fractional domain. For a system with a 28 G baud rate, the FO is usually in the range of $[-5$ GHz, 5 GHz$]$, so we simulate the FO from -5 GHz to 5 GHz with a step of 0.5 GHz. The TO is set to be 4000 symbols. Fig. 9 gives the estimation errors for each modulation format, the absolute values of estimation errors are less than 2 MHz, whose accuracy is high enough for practice application but its estimation range is larger compared with the conventional Viterbi-Viterbi method [26]. In theory, the estimation range of our method is approximately $[-R_s/2, +R_s/2]$. It should be noted that in the TO estimation process, both TO and FO will move to the peak position [20]. Hence large FO will induce the failure of TO estimation, which constrains the FO estimation range. In our simulations, p_{TO} is set to be 0.05 and maximum TO is ± 4096, so the TO induced maximum peak deviation is ± 322 according to Eq. (17). That means the FO estimation range is $[-0.4818R_s, +0.4818R_s]$ when a TO of 4096 symbols is in existence, which is also close to the theoretical interval.

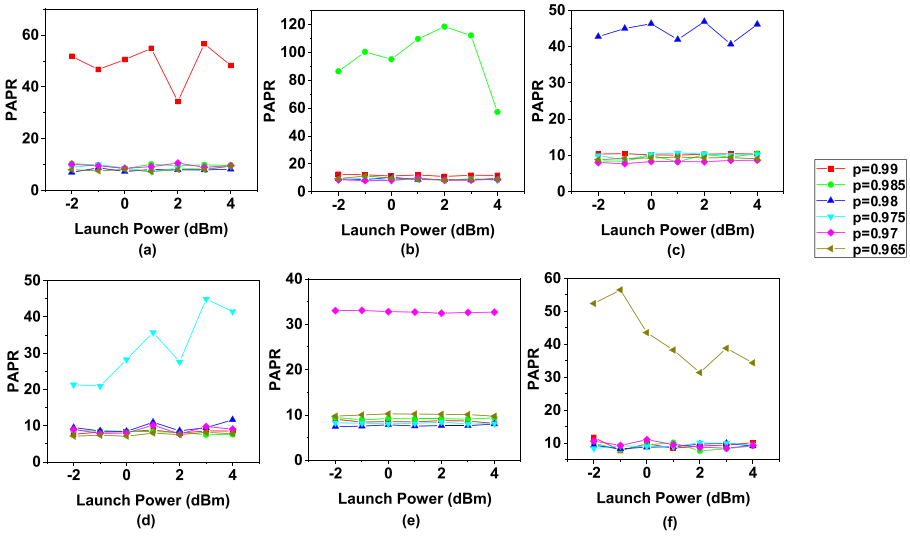

Fig. 8. The PAPR values versus launch powers for (a) DPBPSK; (b) DPQPSK; (c) DP8PSK; (d) DP16QAM; (e) DP32QAM; (f) DP64QAM.

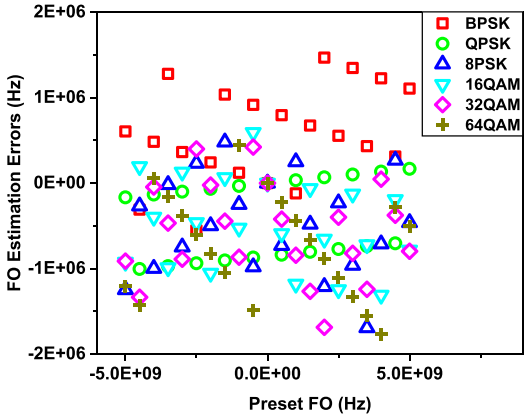

Fig. 9. FO estimation errors for the six modulation formats when FO is in the interval $[-5\ \text{GHz}, 5\ \text{GHz}]$.

3.6 CD Impact Analysis

It is worth noting that massive CD will change the order of LFM signal. In this section, we talk about the CD impact on the LFM signal order. Eq. (7) gives the chirp rate of a p order LFM signal, and the chirp rate will change into $k/(1+2\beta_2 zk\pi)$ after considering CD effects, where k is the original chirp rate, z is the transmission distance, β_2 is the group velocity dispersion (GVD) parameter. According to the relation between the LFM signal order and chirp rate, the chirp rate p' after considering CD effects can be recorded as:

$$p' = \frac{2}{\pi}\left[\arctan\left(\frac{kT}{(1+2\beta_2 zk\pi)\cdot Baud}\right)\right] \tag{18}$$

The CD impact on the order of LFM signal is also discussed by simulation experiments. Fig. 10(a) depicts the order of LFM signal in presence of 32000 ps/nm CD when the LFM signal length is 512 and 16384 symbols. We found the CD will take more influence on the shorter duration LFM signal than the one with longer duration under same original orders which agrees well with the theoretical analysis according to Eq. (18). As is shown in Fig. 10(b) further, for the signal with 16384 symbols, the orders are not changed at all when the value is in $[-0.1, 0.1]$ even CD is up to 320000 ps/nm.

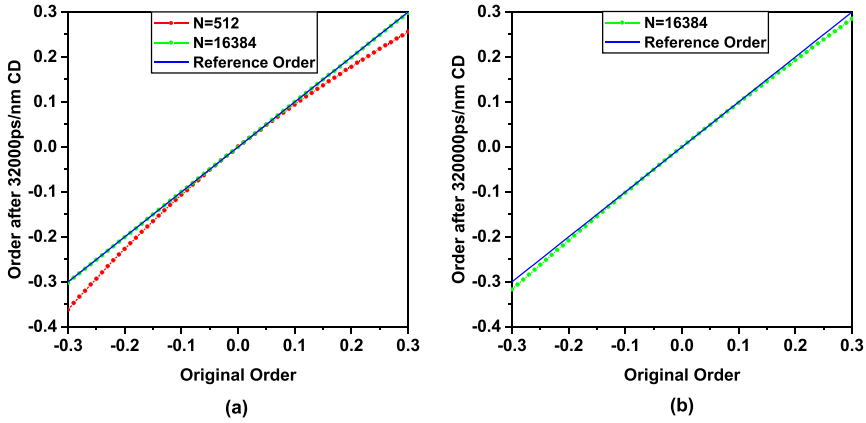

Fig. 10. LFM orders in presence of 32000 ps/nm CD (a) and 320000 ps/nm CD (b).

It verifies that CD takes neglectable impact on the order of the LFM signal with long duration in our scheme.

3.7 Complexity Analysis

Three parts including synchronization, MFI and FO estimation are considered for the complexity analysis. Synchronization can be divided into two steps. First step is finding the rough location of frame head and TO estimation, which can also be referred to as coarse synchronization. The second step is precise synchronization after CD compensation. At the receiver, the rough location of frame head can be determined by scanning the received signal step by step to find the peak after a $1 - p_{TO}$ order FrFT. The scanning block contains N symbols (N is the length of one LFM signal and is set to be 16384 in our simulations) and the step size is set to $N/2$ to ensure the frame head location can be found in a low OSNR. So 8 times FrFTs should be performed to obtain the rough location of frame head. In addition, FrFT is needed one more time to estimate the TO. Until now, the superimposed LFM signal to different modulation formats can be extracted. For the system we present in this paper, 6 times FrFTs should be done for 6 modulation formats and FO estimation. Therefore, FrFTs are performed 15 times totally in our proposal, which consumes $15 \times 16384 \times \log(16384) = 3440640$ multipliers. The follow-up synchronization also needs extra $(2 \times 20 + 1) \times 2^7 = 5248$ multipliers for the TO estimation error of less than 20 symbols. Therefore, 3445888 multipliers are needed in total and only $6 \times 16384 \times \log(16384) = 1376256$ multipliers are for MFI and FO estimation. In contrast, $65536 \times 2^7 = 8388608$ multipliers should be prepared for just the synchronization by traditional algorithm [21]. Clearly, our method uses less multipliers to accomplish more tasks while the traditional method only finishes one task but consumes more multipliers. Hence the computation complexity is obviously reduced by our method.

4. Conclusion

In this paper, we used the LFM signal obtained by operating FrFT on a DC signal to mark and identify the modulation formats. With the aid of deviation between the peak and the middle position in fractional domain, the FO has been estimated simultaneously. Due to the low power, the OSNR penalty at the FEC threshold induced by the superimposed LFM signal is less than 0.5 dB for low order modulation formats and still acceptable for higher order modulation formats, which indicates our method is feasible absolutely in practice. Numerical simulations indicate that the MFI method is still valid even the OSNR is in a very low regime. Moreover, the FO estimate range is approximately extended to $[-R_s/2, +R_s/2]$ in theory with 2 MHz maximum estimation error when FO is in the range of $[-5$ GHz, 5 GHz$]$.

References

[1] O. Gerstel, M. Jinno, A. Lord, and S. B. Yoo, "Elastic optical networking: A new dawn for the optical layer?" *IEEE Commun. Mag.*, vol. 50, no. 2, pp. s12–s20, Feb. 2012.

[2] I. Tomkos, S. Azodolmolky, J. Sole-Pareta, D. Careglio, and E. Palkopoulou, "A tutorial on the flexible optical networking paradigm: State of the art, trends, and research challenges," *Proc. IEEE*, vol. 102, no. 9, pp. 1317–1337, Sep. 2014.

[3] F. N. Khan, K. Zhong, W. H. Al-Arashi, C. Yu, C. Lu, and A. P. T. Lau, "Modulation format identification in coherent receivers using deep machine learning," *IEEE Photon. Technol. Lett.*, vol. 28, no. 17, pp. 1886–1889, Sep. 2016.

[4] J. Liu *et al.*, "Signal power distribution based modulation format identification for coherent optical receivers," *Opt. Fiber Technol.*, vol. 36, pp. 75–81, 2017.

[5] R. Boada, R. Borkowski, and I. T. Monroy, "Clustering algorithms for stokes space modulation format recognition," *Opt. Exp.*, vol. 23, no. 12, pp. 15 521–15 531, 2015.

[6] T. Bo, J. Tang, and C. C.-K. Chan, "Blind modulation format recognition for software-defined optical networks using image processing techniques," in *Proc. Opt. Fiber Commun. Conf. Exhib.*, 2016, pp. 1–3.

[7] X. Mai *et al.*, "Stokes space modulation format classification based on non-iterative clustering algorithm for coherent optical receivers," *Opt. Exp.*, vol. 25, no. 3, pp. 2038–2050, 2017.

[8] L. Jiang *et al.*, "Blind density-peak-based modulation format identification for elastic optical networks," *J. Lightw. Technol.*, vol. 36, no. 14, pp. 2850–2858, Jul. 2018.

[9] W. Zhang *et al.*, "Identifying modulation formats through 2d stokes planes with deep neural networks," *Opt. Exp.*, vol. 26, no. 18, pp. 23 507–23 517, 2018.

[10] D. Wang *et al.*, "Intelligent constellation diagram analyzer using convolutional neural network-based deep learning," *Opt. Exp.*, vol. 25, no. 15, pp. 17150–17166, 2017.

[11] D. Wang *et al.*, "Modulation format recognition and OSNR estimation using CNN-based deep learning," *IEEE Photon. Technol. Lett.*, vol. 29, no. 19, pp. 1667–1670, Oct. 2017.

[12] J. Zhang, W. Chen, M. Gao, Y. Ma, Y. Zhao, and G. Shen, "Intelligent adaptive coherent optical receiver based on convolutional neural network and clustering algorithm," *Opt. Exp.*, vol. 26, no. 14, pp. 18684–18698, 2018.

[13] M. Xiang *et al.*, "RF-pilot aided modulation format identification for hitless coherent transceiver," *Opt. Exp.*, vol. 25, no. 1, pp. 463–471, 2017.

[14] S. Fu *et al.*, "Modulation format identification enabled by the digital frequency-offset loading technique for hitless coherent transceiver," *Opt. Exp.*, vol. 26, no. 6, pp. 7288–7296, 2018.

[15] A. Yang, X. Liu, and X. Chen, "A FrFT based method for measuring chromatic dispersion and SPM in optical fibers," *Opt. Fiber Technol.*, vol. 34, pp. 59–64, 2017.

[16] W. Wang, Y. Qiao, A. Yang, and P. Guo, "A novel noise-insensitive chromatic dispersion estimation method based on fractional Fourier transform of LFM signals," *IEEE Photon. J.*, vol. 9, no. 1, Feb. 2017, Art. no. 7100312.

[17] H. Zhou *et al.*, "Fractional fourier transformation-based blind chromatic dispersion estimation for coherent optical communications," *J. Lightw. Technol.*, vol. 34, no. 10, pp. 2371–2380, May 2016.

[18] A. Yang, P. Guo, W. Wang, Y. Lu, and Y. Qiao, "Joint monitoring of chromatic dispersion, osnr and inter-channel nonlinearity by LFM pilot," *Opt. Laser Technol.*, vol. 111, pp. 447–451, 2019.

[19] W. Wang, A. Yang, P. Guo, Y. Lu, and Y. Qiao, "Joint OSNR and interchannel nonlinearity estimation method based on fractional Fourier transform," *J. Lightw. Technol.*, vol. 35, no. 20, pp. 4497–4506, Oct. 2017.

[20] H. Zhou *et al.*, "Joint timing/frequency offset estimation and correction based on FrFT encoded training symbols for PDM CO-OFDM systems," *Opt. Exp.*, vol. 24, no. 25, pp. 28256–28269, 2016.

[21] H. Jiang *et al.*, "Joint time/frequency synchronization and chromatic dispersion estimation with low complexity based on a superimposed FrFT training sequence," *IEEE Photon. J.*, vol. 10, no. 5, Oct. 2018, Art. no. 7203710.

[22] H. M. Ozaktas, O. Arikan, M. A. Kutay, and G. Bozdagt, "Digital computation of the fractional Fourier transform," *IEEE Trans. Signal Process.*, vol. 44, no. 9, pp. 2141–2150, Sep. 1996.

[23] A. W. Lohmann, "Image rotation, wigner rotation, and the fractional Fourier transform," *J. Opt. Soc. Amer. A*, vol. 10, no. 10, pp. 2181–2186, 1993.

[24] G. Liu, R. Proietti, K. Zhang, H. Lu, and S. B. Yoo, "Blind modulation format identification using nonlinear power transformation," *Opt. Exp.*, vol. 25, no. 25, pp. 30895–30904, 2017.

[25] M. Xiang *et al.*, "Modulation format identification aided hitless flexible coherent transceiver," *Opt. Exp.*, vol. 24, no. 14, pp. 15642–15655, 2016.

[26] M. Morelli and U. Mengali, "Feedforward frequency estimation for psk: A tutorial review," *Eur. Trans. Telecommun.*, vol. 9, no. 2, pp. 103–116, 1998.